The Role of Lanthanum in a Nickel Oxide‐Based Inverted Perovskite Solar Cell for Efficiency and Stability Improvement

The role of lanthanum on a nickel oxide-based inverted perovskite solar cell for efficiency and stability improvement

Siowhwa Teo,*[a] Zhanglin Guo,[a] Zhenhua Xu,[a] Chu Zhang,[a] Yusuke Kamata,[a] Shuzi Hayase,[a] Tingli Ma*[a]

Abstract: A high performing inverted perovskite solar cell (PSC) always relies on the hole transporting layer (HTL) quality and its interfaces. This work is the first to investigate the impact of lanthanum (La) incorporation within the NiO_x matrix for defects passivation, thus lead to high charge extraction ability and stability without compromising its power conversion efficiency. In the presence of La, the La-NiO_x quality is obviously improved; without the formation of pinholes. In addition, the inclusion of La alters the energy band alignment; consequently, enhances the hole transportation and widens the V_{oc} (> 1V), as compared to the pristine NiO_x. The beneficial effect of La is further revealed through the PL measurement and density of states (DOS) analysis, where trap states are passivated by La. More importantly, the perovskite solar cell, with La-NiO_x as the HTL, exhibits 21% enhancement in efficiency and a remarkable stability than that of pristine NiO_x. This also unlocks another opportunity for commercialization.

Introduction

Considerable attention has been focused on engineering a perovskite solar cell (PSC) with the highest efficiency and stability in order to realize practical usage for the development of a future green environment.[1-3] To achieve the stability accomplishment, the used of the inorganic hole transport layer (HTL) such as NiO has indeed substantially improved the stability and lifetime of the solar cell upon replacing the commonly used organic HTL (Spiro-OMeTAD or PEDOT:PSS). Taking an example, Rong et al. reported that the solar cell device composed of NiO HTL exhibited excellent stability under light soaking condition.[4] More importantly, the NiO renders high hole mobility (10^{-15} to 10^{-3} $cm^2V^{-1}s^{-1}$),[5] wide bandgap (E_g > 3.5 eV) which resulted in low absorption losses, high conduction band edge to perform as efficient electron blocker, and improved lifetime than the PEDOT:PSS and spiro-OMeTAD, which are the key factors to boost the power conversion ability of the solar cell.[6-8] The well-aligned energy levels of NiO resulted in higher open circuit voltage (V_{oc}) and better device performances, in comparison to the PEDOT:PSS-based devices.[6,9]

However, the low intrinsic conductivity of NiO has resulted in an accumulation of hole near the perovskite interface, increased recombination rate, and reduced charge collection, which is disadvantaging the photovoltaic performance. Thus, relentless efforts have been performed to improve the conductivity, charge collection ability, and the film quality of the NiO either through the employment of different deposition methods or by introducing dopants. Thus far, sophisticated and high cost preparation methods such as pulsed laser deposition, high temperature spray pyrolysis, and atomic layer deposition methods have been utilized to improve the quality of NiO film ascribed to a high performing solar cell is always relying on the film's quality.[7,10-12] Huang et al. have demonstrated a PCE of 12.6% for a cobalt-doped NiO_x solar cell by the sputtering method;[13] while 16.4% efficiency was achieved when a uniform NiO_x layer was prepared through the electrochemical deposition process.[11] The conductivity of NiO_x is usually tuned by doping with other elements such as copper,[14] cobalt,[13] or co-doped of lithium and cobalt[15] through stoichiometry adjustment. By introducing copper as the co-dopant within the NiO_x matrix, the PCE was dramatically increased from 8.9% (for undoped NiO_x) to an impressive efficiency of 15.4%, revealing the effectiveness of dopant in promoting the power conversion ability of the solar cell.[16] In addition, the incorporation of cesium (Cs) within the NiO_x lattice improved the transparency of the film, consequently enhances its hole extraction mechanism and PCE[17] and the addition of Cu ions contributed to high PCE of 17.41% for the flexible devices.[18] While, the incorporation of a novel molecular doping 2,2'-(perfluoronaphthalene-2,6-diylidene)dimalononitrile (F6TCNNQ) into NiO_x decreases the energy level offset between the valence band maximum of NiO_x and the perovskite which enhances electron transfer, as verified through electrostatic force microscopy (molecule-doped NiO). The effectiveness of molecular F6TCNNQ-doped NiO_x based PSC was revealed through boosted PCE of ~7%, as compared to the undoped PSC.[19] Zhang et al. introduced a simple post-device ligand treatment which has not merely improves the PCE of the solar cell, but it also greatly improves the stability of the device ascribed to the hydrophobic property of the chemical modified perovskite layer by the ligand vapours.[20] Recently, a researcher has reported an average PCE of 16.3% for an Ag-doped NiO_x based perovskite solar cell. However, its stability has somehow been compromised where 93% efficiency retained after storage in an N_2 box in the dark for 30 days.[21]

In this work, we are the first group to report the photovoltaic performances of a NiO_x based inverted perovskite solar cell using La as the co-dopant owing to its (i) ability to tune the band alignment; (ii) high binding strength to oxygen which is

[a] Dr. Siowhwa Teo, Zhanglin Guo, Zhenhua Xu, Chu Zhang, Yusuke Kamata, Prof. Dr. Shuzi Hayase, Prof. Dr. Tingli Ma

Graduate School of Life Science and System Engineering, Kyushu Institute of Technology, 2-4 Hibikino, Wakamatsu-ku, Kitakyushu, Fukuoka, 808-0196, Japan.

E-mail: siowhwa_teo@hotmail.com; tinglima@life.kyutech.ac.jp

Supporting information for this article is given via a link at the end of the document.

able to scavenge oxygen; and (iii) suppress decomposition of perovskite under light illumination. A simple solution processing route was performed to synthesized the La-NiO_x HTL interlayer for the device configuration of FTO/La:NiO_x/$CH_3NH_3PbI_3$/$PC_{61}BM$/BCP/Ag. We found that with the presence of La, the film quality of the $CH_3NH_3PbI_3$ perovskite is highly improved than that of pristine NiO_x, consequently prompted for high PCE over 15% with high V_{oc} exceeding 1 V. It is confirmative that the as-synthesized La-NiO_x HTL is highly uniform and is highly reproducible. The beneficial effects of the La are further being revealed through its superior charge extraction capability, compatible energy alignment, and improved PL quenching effectiveness. From the PL measurement, we can assure that the incorporation of an optimum amount of La has reduced the trap density, subsequently improve the charge transportability of the cell. Impressively, the La-NiO_x solar cell exhibits remarkable stability even after storage in a vacuum desiccator for 50 days.

Results and Discussion

In this work, we focus on the fabrication and performance of a La-NiO_x inverted perovskite solar cell (PSC) composed of FTO/NiO_x/$CH_3NH_3PbI_3$/$PC_{61}BM$/BCP/Ag, in which

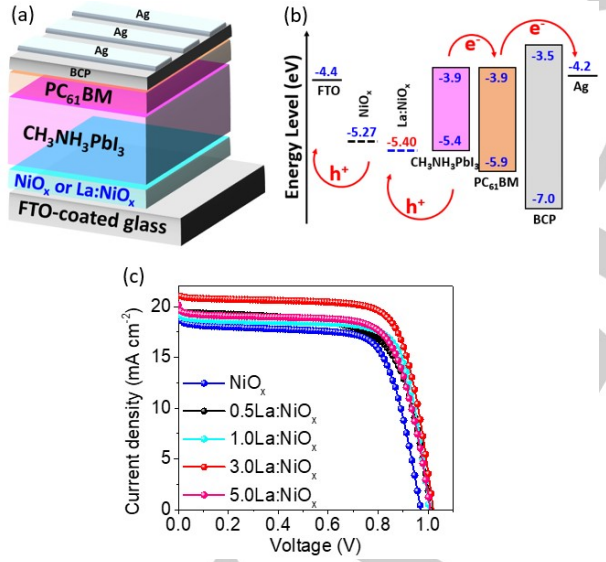

Figure 1. (a) Device construction of the inverted planar perovskite solar cell (PSC). (b) Scheme energy diagram of FTO/HTLs/$CH_3NH_3PbI_3$/$PC_{61}BM$/BCP/Ag device showing the energy level of each layers, both pristine and La-HTLs were calculated from PYS analyses. (c) Current density-voltage (*J-V*) characteristic of the PSCs with different La content in La-NiO_x measured under standard test conditions (AM1.5G, 100 mW cm^{-1}), all the measurements were performed in ambient air without encapsulation (relative humidity of ≈50-70%).

the pure NiO_x films were synthesized through a simple solution-based route,[22] while the La-NiO_x (La:NiO_x) films were prepared by incorporating La precursors ($LaCl_3$) at a molar ratio ranging from 0.5–5 mol%. The device architecture of the inverted planar PSCs is revealed in **Figure 1a**. The NiO_x or La-NiO_x and phenyl-C61-butyric acid methyl ester ($PC_{61}BM$) are selected as the HTL and electron extracting layer (EEL), respectively. While bathocuproine (BCP) acts as an interface layer at the cathode side to reduce energy barrier for electron extraction.[23] The $CH_3NH_3PbI_3$ perovskite films were fabricated by facile one-step solvent engineering process with some modifications.[22] **Figure 1b** summarizes an energy level diagram. The valence band of La-NiO_x is deeper than the FTO, which suggests the efficient injection of holes from the HTL to FTO. The *J-V* curves and the dependence photovoltaic parameters of various La concentrations are presented in **Figure 1c and Figures 2a-d**, and their photovoltaic performances are summarized in **Table 1**. It can be concluded that the best device

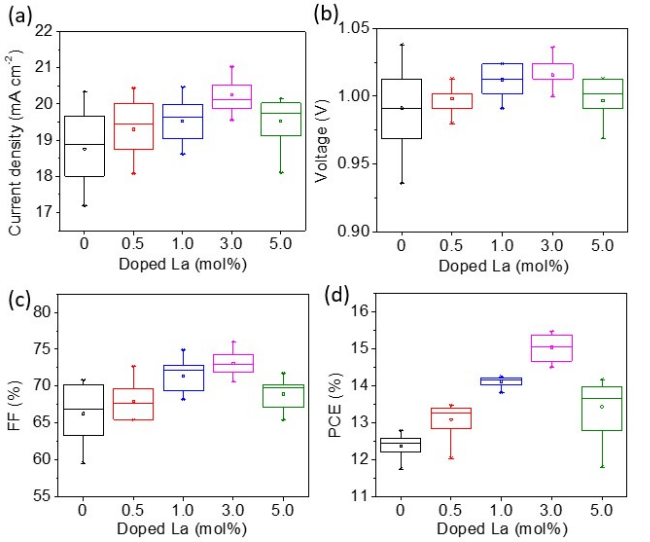

Figure 2. (a-d) Dependence of photovoltaic parameters of the NiO_x and La-NiO_x perovskite devices on La contents.

is produced from La-NiO_x of 3 mol% with a high PCE of 15.46%, which is 1.25-fold higher than the pristine NiO_x film. Therefore, 3 mol% of La is chosen for further in-depth study in this paper.

For optical properties evaluation, both the pristine and La-NiO_x thin films on quartz revealed good optical transmittance above 80 % ranging from 350 to 800 nm, as illustrates in **Figure 3a**. The extremely high transparent HTLs, as compared to the bare FTO glass, enables the reaching of light to the perovskite interface for high photocurrent generation, which is an essential criterion to surge excellent power output for a solar cell. The work function of the NiO_x and La-NiO_x thin films were determined using photoelectron yield spectroscopy (PYS), as shown in **Figure 3b**. The La-NiO_x component had a deeper work function of 5.40 eV than the NiO_x component (5.17 eV), and the closer

work function of La-NiO_x to the valence band of $CH_3NH_3PbI_3$ (5.4 eV) thus favors the hole transportation **(Figure 1c)**. Moreover, the deeper work function of La-NiO_x theoretically enhances the V_{oc} of the device due to a wider potential difference between the valence band (VB) of NiO_x and the conduction band (CB) of perovskite.[24] As a result, La doping resulted in excellent hole extraction across the perovskite-NiO_x-HTL interfaces.

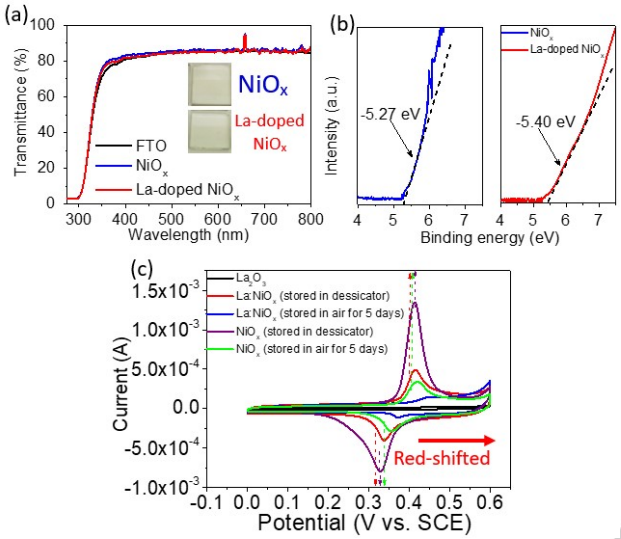

Figure 3. (a) Transmission spectra of NiO_x and La-NiO_x HTL coated on FTO glass, the insert shows the corresponding photographs of both films. (b) The PYS spectrum of the NiO_x and La-NiO_x thin films coated on quartz substrates. Cyclic voltammetry of various HTLs fabricated on FTO glass substrate.

The stability, durability, and resistivity of La-NiO_x and pristine NiO_x are evaluated through the cyclic voltammetry (CV) scanning from 0-0.6 V in a 2M KOH electrolyte using a three-electrode system, as depicted in **Figure 3c**. The CV profile displays a distinct pair of redox peaks during the anodic and cathodic sweeps, indicative of the oxidation of NiOOH to NiO (charging) and the reduction of NiOOH to NiO (discharging), as in accordance to equation (1):

$$NiO + OH^- \leftrightarrow NiOOH + e^- \quad (1)$$

Two intense electrochemical redox peaks of NiO are observed at 0.3 and 0.4 V, imply the occurrence of reversible redox Faradaic processes of Ni^{2+} to Ni^{3+} during the oxidation and Ni^{3+} to Ni^{2+} during the reduction processes.[25] The presence of La^{3+} within the NiO_x framework is proven through the obvious reduction of redox peak's intensity (red cyclic voltammogram) and the insignificant change of CV shape of La-NiO_x from the pristine NiO_x indicates good charge conduction of the La^{3+} in the host materials. Importantly, the addition of La^{3+} enhances the stability of La-NiO_x, as opposed to the pristine NiO_x. Comparatively, the intensity of the pristine NiO_x redox peak plunged significantly (1 order of current magnitude reduced from 10^{-3} to 10^{-4} A) upon keeping the pristine NiO_x substrate outside the desiccator. In contrast, the La-NiO_x shows negligible degradation after stored outside of the desiccator for 5 days.

The crystallinity of the synthesized NiO_x and La-NiO_x thin films using solution engineering route are both evaluated through X-ray diffraction (XRD) techniques. The XRD spectra of **Figure 4a** and **Figure S1** demonstrate all peaks can be indexed to NiO_x and no other extra peaks are found, indicate high purity NiO_x has been obtained. The weak intensity diffraction peaks of the NiO_x situated at 37.24º, 42.38º, and 62.86 are well correspond to the cubic *Fm*3*m* crystal structure and are indexed to (111), (200), and (220) planes of the NiO (JCPDS File No.: 47-1049). Similar XRD patterns are also observed for HTLs coated on quartz substrates **(Figure S1)**, which indicate that the NiO_x crystal that synthesized from solution had week polycrystallinity.[10] There is no change on the XRD peaks or no extra peaks that can be assigned to La^{3+} **(Figure 4a and Figure S1)** even the dose of La^{3+} has been increased, indicates that the doping metal ion is not substituting the NiO_x crystal lattice ions and the La^{3+} ions are homogeneously dispersed in the gel matrix without any segregation,[26,27] which further enhance the electrochemical activity of the material.

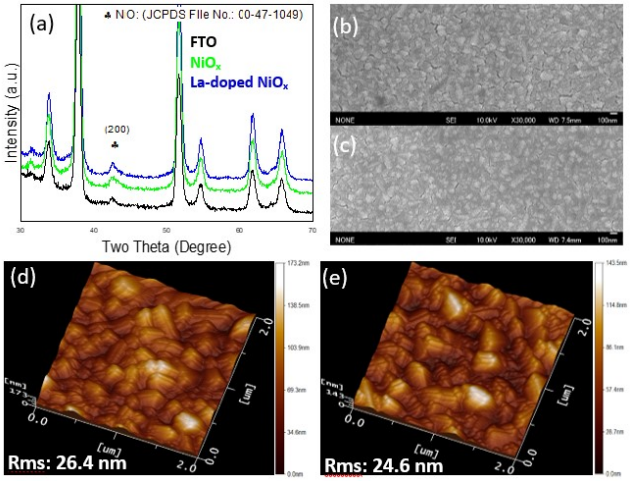

Figure 4. (a) XRD patterns of FTO substrate, NiO_x and La-NiO_x thin films coated on FTO glass after thermal annealing. Morphology of the NiO_x, La-NiO_x HTL and perovskite films: SEM images of (b) NiO_x and (c) La-NiO_x on FTO glass, the scale bar is 1 µm. (d,e) 3D AFM images of the corresponding NiO_x and La-NiO_x thin films, the scan size is 2 x 2 µm.

Notably, the performance of the perovskite solar cell is highly dependent on the morphological surface of the perovskite film. The enhancement of La-NiO_x addition from the

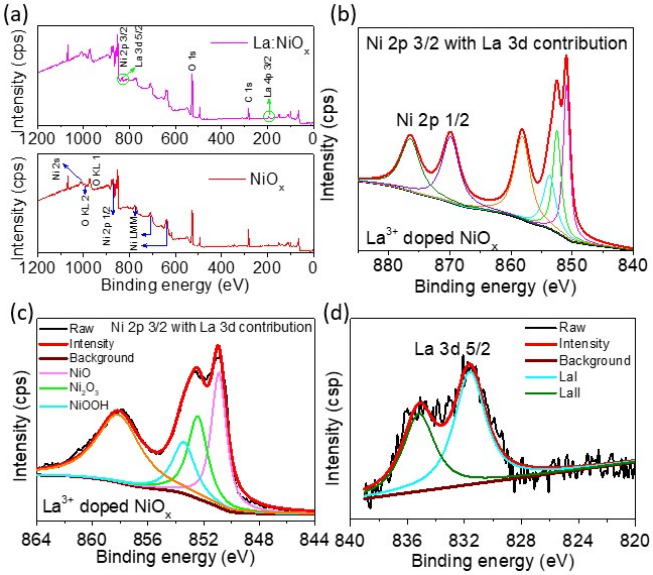

Figure 5. (a) Wide scan of XPS survey spectrum of NiO_x and La-NiO_x thin films. (b,c) High resolution of XPS profiles of Ni 2p core level, corresponding to the Ni and La elements in the La-NiO_x thin films. (d) La 3d 5/2 XPS spectra of La-NiO_x.

aspect of its morphological structure is depicted from the 3D atomic force microscopy (AFM) and scanning electron microscopy (SEM), respectively. The compactness of the La:NiO_x was improved (without any pinholes), as compared to the pristine NiO_x, which consequently led to the formation of a pinhole-less perovskite film, as observed from **Figure 4b, Figure 4c,** and **Figure S3**. In great agreement with the SEM images, **Figure 4d** and **Figure 4e** of the AFM analysis revealed that the La-NiO_x displays a smoother surface (RMS = 24.6 nm) than the pristine NiO_x (RMS = 26.4 nm), which led to the growth of large perovskite granules in the size range of 200-500 nm (**Figure 6a** and **Figure 6b**). The smooth surface of La-NiO_x enhanced the growth and quality of the perovskite film (pinhole-free) owing to the inclusion of small amount of La on the NiO_x which acts as a growing seed site that influence the nucleation process of the perovskite, consequently favors the growth of highly dispersed nuclei. Comparatively, the pristine NiO_x possesses smaller perovskite granules in the size of 100-350 nm, which disfavoured the charge transport properties.

X-ray photoelectron spectroscopy (XPS) has been performed to confirm the presence of La^{3+} within the NiO_x matrix, as shown in **Figure 5** and **Figure S2**. The binding energies are corrected by referencing the C1s peak to 284.8 eV. The wide scan in **Figure 5a** proofs the presence of La within the NiO_x matrix; showing the peaks at 834.3 eV and 197.9 eV, which corresponds to La3d and La4p (green circles). Likewise, from the narrow scan, two deconvoluted peaks with a binding energy of 834.2 eV (LaI) and 837.8 eV (LaII) are observed from the La3d spectrum, indicate the presence of La. While six deconvoluted peaks are observed from the Ni2p spectrum **(Figure 5a,b** and **Figure S2a,b)**. The binding energy of Ni remains un-shifted, which hypothesized that the La^{3+} is not incorporated into NiO crystal lattice in the case of La-NiO_x thin film.[28] This result is consistent with the results obtained from XRD analysis. The peak situated at 860.8 eV in the Ni2p spectrum **(Figure 5c, and Figure S2b)** was ascribed to the shake-up process of NiO_x. In addition, the peak at a binding energy of 853.5 eV represents the presence of Ni in an oxidation state of +2; while the binding energy at 855 eV and 856.1 eV represent Ni^{3+} that was induced by the vacancy in Ni_2O_3 and the presence of NiOOH, respectively. In contrast, La-NiO_x thin film exhibits higher Ni^{3+}/Ni^{2+} ratios that could increase the hole conductivity of NiO_x film and improve the contact properties of the solar cells.[29,30] This result has further revealed the merit point of La for improved film quality and crystallinity.[31]

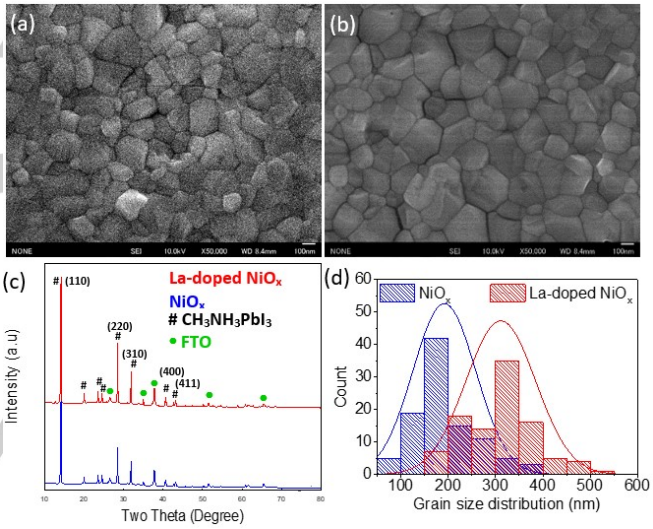

Figure 6. Top view SEM images of the perovskite films deposited on the (a) NiO_x and (b) La-NiO_x thin films. (c) XRD patterns of perovskite films deposited on the NiO_x and La-NiO_x thin films. (d) Grain size distribution of the corresponding of perovskites grown on NiO_x and La-NiO_x thin films.

It has been reported that the performance of a perovskite device is always correlated to the film morphology, film crystallinity, and crystal size, etc. In this study, we adopted a modified one-step deposition Lewis acid-base adduct approach for high-efficiency and quality $CH_3NH_3PbI_3$ film formation. During the 5th second of spin-coating, a non-polar CB was spin-casted on top of the $CH_3NH_3PbI_3$ in order to form a thick adduct-induced $CH_3NH_3PbI_3$ film, which is hypothesized to be in pure phase and large crystal grains by slowing down the perovskite crystallization rate.[32] To verify our hypothesis, as shown in **Figure 6a, Figure 6b** and **Figure S3**, the La-NiO_x thin film is indeed perfectly covered by the $CH_3NH_3PbI_3$ film; with dense

and large crystallized grains, which is similar to that of NiO_x thin film. The only difference between the perovskite grown on La-NiO_x and pristine NiO_x is its crystallize sizes. The perovskite film grown on a smoother La-NiO_x's surface exhibited larger average grain size (in the range of 200-500 nm), which in turn resulted in the formation of highly compact perovskite layer than the pure NiO_x (in the range of 100-350 nm).

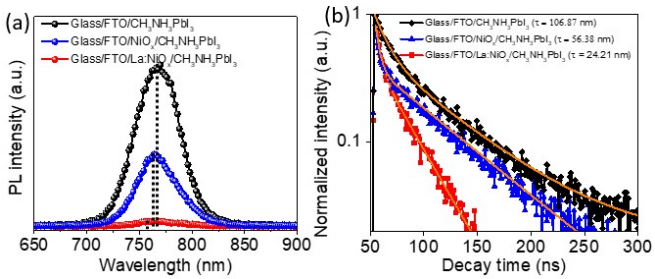

Figure 7. (a) steady state photoluminescence (PL) and (b) time resolved PL spectra for perovskite films on different substrates: FTO (black), NiO_x (blue) and La-NiO_x (red).

This phenomenon assures that the growth of a high quality perovskite film is highly relying on the bottom layer (NiO_x). Meanwhile, XRD profiles reveal that both absorbance films demonstrated intense diffraction peaks at 2θ value of 14.3°, 20.0º, 23.6º, 24.6º, 28.5°, 31.9º, 35.1º, 40.7º, and 43.5º, which corresponding to the (110), (200), (211), (220), (320), (310), (321), (400), and (411) crystal planes of the $CH_3NH_3PbI_3$ with an orthorhombic *Pnma* crystal structure, respectively. The X-ray diffraction peak intensity of $CH_3NH_3PbI_3$ on different HTL layers is significantly different. The peak intensity of $CH_3NH_3PbI_3$ is much higher when deposited on La-NiO_x, as compared to the NiO_x HTLs. The growing of highly crystallized $CH_3NH_3PbI_3$ film on the La-NiO_x film, relative to the pristine NiO_x film has thus merited the charge transport and charge extraction, and also enhanced J_{sc} of La-NiO_x HTL based devices. The vast difference in XRD peak intensities of $CH_3NH_3PbI_3$ on different HTL layers imply the improved crystallinity of $CH_3NH_3PbI_3$ film on La-NiO_x film, as compared to the pristine NiO_x film, which is responsible for J_{sc} enhancement for the La-NiO_x HTL based device.

In addition, the steady-state (SS) and time-resolved (TR) PL spectra of $CH_3NH_3PbI_3$ interfaced with HTL-free, NiO_x, and La-NiO_x films were evaluated to assess the effect of La towards the charge transport and charge extraction efficiencies of the HTLs/ $CH_3NH_3PbI_3$. As illustrated in **Figure 7a**, the SSPL peak was slightly blue-shifted from 768 nm ($CH_3NH_3PbI_3$ film on top of FTO glass) to 763 nm upon the incorporation of La^{3+}, while a peak situated at 761 nm is assigned to the pristine NiO_x. The blue-shifted SSPL of La-HTL perovskite implies the effective passivation of trap states by the La^{3+} ions, which is attributed to the improved perovskite film quality and crystallinity.[33] The effective passivation effect of La^{3+} ions is further revealed through the density of states (DOS) and Bode phase analysis, as depicted in **Figure S4a** and **Figure S4b**. The DOS distribution of La-NiO_x HTL obtained from PYS is lower than that of pristine NiO_x, implies the effective passivation of trap states by the La. In addition, the frequency peak of the La-NiO_x observed from the Bode plot shifted to a lower frequency region, implies a longer electron lifetime and excellent charge transport mechanism. In addition, the effective passivation effect and high crystallinity of the La-HTL perovskite film enhance the visible light absorption ranging from 400 to 750 nm **(Figure S5)**, as opposed to the $CH_3NH_3PbI_3$/FTO and $CH_3NH_3PbI_3$/NiO_x. The absorption band edges for both perovskite films (with and without La) are perfect matches, indicating that the total amount of perovskite loaded in each case is identical.[34]

To further investigate the carrier dynamics of the perovskite material coated on La- or pristine NiO_x, TRPL decay time curve **(Figure 7b)** was performed and was fitted to a phenomenological double exponential decay model as in following:[35]

$$I(t) = I_0 + B_1 \exp\left(-\frac{t-t_0}{\tau_1}\right) + B_2 \exp\left(-\frac{t-t_0}{\tau_2}\right) \quad (2)$$

While the average decay times were determined by using the equation as shown below:

$$\tau_{Avg.} = \frac{\sum B_i \tau_i^2}{\sum B_i \tau_i} \quad (3)$$

where the fast decay time constant τ_1 reflects the diffusion of the photogenerated excitons into defects. Whilst, the slow time constant τ_2 is associated with the radiative exciton lifetime of $CH_3NH_3PbI_3$ on HTL. [7] The lifetime of HTL-free $CH_3NH_3PbI_3$ film is approximately 106.87 ns and is significantly reduced to 56.28 ns when the $CH_3NH_3PbI_3$ was deposited on pure solution process NiO_x hole interlayer, indicating that the photogenerated charge carriers are effectively transported to NiO_x HTL **(Table 2)**.

Table 1. Summary of the photovoltaic parameter of the inverted planar PSCs with NiO_x and La-NiO_x HTLs. The values were calculated from 15 devices.

La cons. [mol%]	J_{sc} [mA cm^{-2}]	V_{oc} [V]	FF [%]	PCE [%]
0	18.76 ± 0.98	0.99 ± 0.042	66.69 ± 3.4	12.32 ± 0.42
0.5	19.90 ± 0.79	1.00 ± 0.012	68.00 ± 2.3	13.08 ±0.41
1.0	19.53 ± 0.58	1.01 ± 0.011	71.34 ± 2.3	14.09 ± 0.20
3.0	20.25 ± 0.47	1.02 ± 0.013	73.10 ± 1.5	15.03 ± 0.34
5.0	19.53 ± 0.60	1.00 ± 0.016	68.90 ± 2.1	13.41 ±0.74

While, when the La^{3+} was incorporated into the NiO_x matrix, the lifetime is further dramatically reduced (2.3-fold decrement) to 24.21 ns from that of pure NiO_x. Concluded from the hall measurement **(Table S1)**, it is hypothesized that the carrier density of the La-NiO_x HTL decreases from 3.92x10^{14} cm^{-3} (pristine NiO_x) to 2.32x10^{10} cm^{-3} where this result is in great agreement with the energy band shift data obtained from PYS. The addition of La has downshifted the band structure **(Figure**

1b), which favors the hole extraction process. In addition, the La-NiO_x HTL exhibited 2.3-fold higher in mobility (59.01 $cm^2V^{-1}s^{-1}$) than that of the pristine NiO_x HTL (26.09 $cm^2V^{-1}s^{-1}$); gave rise to long diffusion length exceeding ~ 2 µm. This phenomenon has provided evidence that the perovskite with La-NiO_x indeed exhibits excellent charge extraction ability, fewer recombination sites, and trap states than the pristine perovskite. Therefore, in accordance to all the characterized results obtained (as have been discussed earlier), we can conclude that obtaining a highly compact, pinhole-free, and highly crystalline HTL (in our case it refers to NiO_x or La-NiO_x) are important for efficient hole transfer between perovskite and NiO_x layers, in addition to excellent charge extraction and collection in an inverted perovskite solar cell.[36]

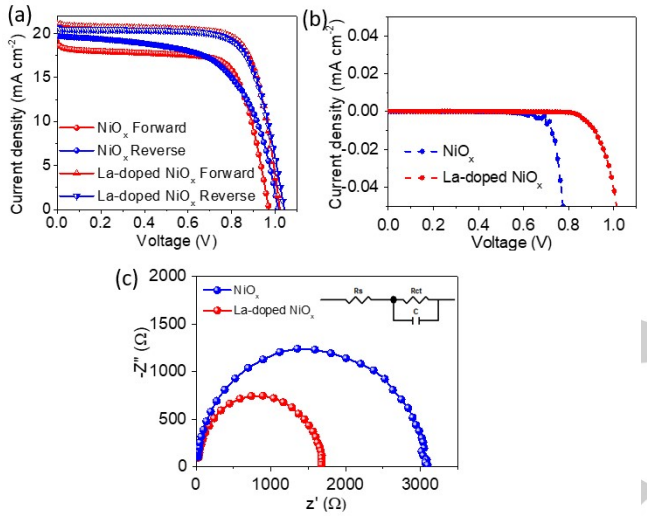

Figure 8. (a) J-V curve of perovskite solar cells based on different hole extraction interlayers, data collected in the forward scan direction. (b) Stabilized photocurrent density (red) and PCE (blue) measured at maximum power voltage of 0.84 V for 150 s. (b) J-V measured under dark conditions. (c) EIS spectra for Glass/FTO/NiO_x/$CH_3NH_3PbI_3$/$PC_{61}BM$/BCP/Ag and Glass/FTO/La:NiO_x/ $CH_3NH_3PbI_3$/$PC_{61}BM$/BCP/Ag cells measured in dark with a bias of 0.8 V.

The photovoltaic performances of the La-NiO_x perovskite solar cell are investigated, as shown in **Figure 8** and the photovoltaic parameters are summarized in **Table S2**. The PSCs device composed of La-NiO_x HTL exhibited a promising PCE of 15.46 % with a V_{oc} of 1.01 V, J_{sc} of 21.02 mA cm^{-2}, and a fill factor (FF) of 0.73, which is 21% higher than the pristine NiO_x HTL device which with a PCE of 12.79 % (V_{oc}, J_{sc}, and FF were 0.79 V, 19.66 mA cm^{-2}, and 0.67, respectively). The beneficial effect of doping La is further revealed through the negligible hysteresis effect of only 0.3% difference between the forward and reverse PCE, as observed from the *J-V* curves of **Figure 8a**. While the perovskite device with pristine NiO_x exhibited huge hysteresis due to vast PCE difference between the forward (12.79%) and reverse (12.21%) scan; with a difference of 4.5%. The stable steady-state PCE **(Figure S6a)** of La-NiO_x based device measured over 150 s has recorded a PCE of 15.2 %, which is comparable and consistent to the current density obtained from *J-V* curve (18.8 $mAcm^{-2}$), thus implies its reliability.

Table 2. Summary of the PL lifetime parameters from fitting curves of PL decay measurements.

Devices	B_1 [%]	τ_1 [ns]	B_2 [%]	τ_2 [ns]	Weighted average τ [ns]
Glass/FTO/$CH_3NH_3PbI_3$	545.62	24.51	469.11	125.57	106.87
Glass/FTO/NiO_x/$CH_3NH_3PbI_3$	759.64	3.82	368.70	62.95	56.38
Glass/FTO/La:NiO_x/$CH_3NH_3PbI_3$	723.41	4.35	435.22	29.14	24.21

In addition, the dark current analysis was performed to determine the existence of an—energy barrier at the HTL surface.[37] The dark current of the NiO_x HTL-based device was observed at a low forward bias **(Figure 8b)**, implying that charge recombination is facilitated at the NiO_x/$CH_3NH_3PbI_3$ interface. With La modification, the dark current was consequently shifted to a higher forward bias direction, which may be due to the suppressed backflow of holes, *i.e.*, hole recombination from NiO_x to $CH_3NH_3PbI_3$ layer, which is in good agreement with the high V_{oc} obtained from the La modified device.

Electrochemical impedance spectroscopy (EIS) has been performed to gauge the performance enhancement, charge transfer resistance, and interfacial properties of the as-fabricated PSCs. **Figure 8c** presents the Nyquist plots for all devices measured in dark at an applied bias voltage of 0.8 V from a frequency ranging from 0.1 to 1.0 Hz. The Nyquist plots were fitted using an equivalent circuit model consisting of series resistance (R_s), charge transfer resistance (R_{ct}), and a parallel capacitor (C),[38] as illustrated as an insert in **Figure 8c**. The curve fitting data of both NiO_x and La-NiO_x HTL-based devices are summarized in **Table S1**. The effectiveness of La dopant on photovoltaic enhancement is revealed when the R_{ct} of La-NiO_x based device is significantly reduced (2.6-fold decrement) from 3100 Ω for the pristine NiO_x to 1200 Ω. It is notable that the reduction in internal resistance enhances the conductivity of the hole interlayer, suggests that the charge transfer within the La-NiO_x device is much more efficient with less charge recombination, consequently enhances the J_{sc} of the device. The photovoltaic enhancement of the La-NiO_x HTL-based device is in agreement with the incident photon-to-electron conversion efficiency (IPCE), as shown in **Figure S6b**. A photocurrent of 18.83 mA cm^{-2} is integrated from the IPCE spectra for the La-NiO_x solar cell. The slight reduced J_{sc} could be attributed to the lower illumination intensity during the IPCE measurement, where the recombination process is more prominent due to trap state and space charge effects.[39] Comparatively, the higher IPCE value of La-HTL device, as compared to the NiO_x based HTL device **(Figure S6c)** is ascribed to the improved light absorption ability **(Figure S5)** and the improved photon to electricity conversion efficiency, implies the less occurrence of recombination mechanism within the La-NiO_x film. Evaluating from the photovoltaic aspect, likewise, the increased J_{sc}, V_{oc},

and FF values are credited to the beneficial role of La doping which provides better energy band alignment, enhances film conductivity, and reduces trap states as discussed above. **Table S3** summarizes the photovoltaic performances of our fabricated state-of-art with other reported inverted PSCs. In general, our fabricated La-NiO_x organic-inorganic hybrid inverted PSC demonstrated promising photovoltaic improvement among those reported devices.

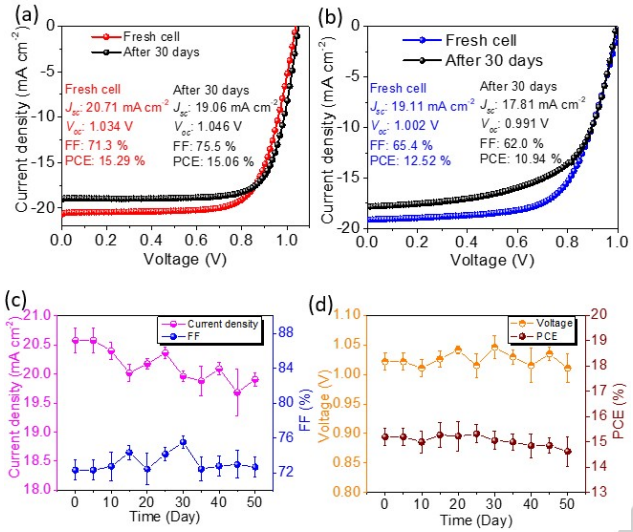

Figure 9. (a) La-NiO_x and (b) NiO_x HTL-based cells, after 30 days storage in glove box. (c,d) Photovoltaic performance parameters of La-NiO_x perovskite cells (five devices) as a function of storage time in moiture-free desiccator for 50 days. (c) *J-V* measurement of the as-prepared devices. All devices were tested without encapsulation. The devices were measured in air and store in moiture-free desiccator during other periods.

To evaluate the stability and reversibility of our fabricated device, the PCE of both La- and pristine NiO_x perovskite solar cells were recorded after 1-month storage in a nitrogen-filled glovebox, as portrayed in **Figure 9a** and **Figure 9b**. The solar cell with La-NiO_x displays a PCE of 98% after 1-month of storage, as compared to the pristine NiO_x device (87% efficiency retained), implies the beneficial effect of La in preventing the undesired oxidation process on the NiO_x surface (as shown in CV profile). To further prove the value of our fabricated architecture, the stability and sustainability of the La-NiO_x HTL-based devices were performed by storing the cells in a moisture-free desiccator without encapsulation for 50 days; while the cells were tested in an ambient environment, as depicted in **Figure 9c** and **Figure 9d**. Impressively, the solar cell with La-NiO_x as the bottom layer displays negligible PCE loss (excellent stability) where 95% of its initial efficiency was still retaining even after 1 month of storage in a moisture-free desiccator. From these results, we can assure that the La dopant is able to stabilize the NiO_x framework, fill the pinholes (consistent with SEM images), and suppress electronic trap states (proven in PL spectrum), consequently boost the photovoltaic performances. Conclusively, the highly stable La-NiO_x HTL behaves as a stable anode interfacial layer, which is one of the best choices for stability achievement. [31,40,41]

Conclusions

In summary, we are the first group to incorporate La within the NiO_x framework, which is not merely boosted the PCE, but also improved the stability of the solar cell for practical usage realization. Impressively, by doping 3 mole % La, the solar cell stored in a moisture-free desiccator displayed remarkable stability (95% efficiency retained) even after storage of 50 days; while 98% efficiency retained for the La-NiO_x solar cell stored in the glovebox, which is far more stable than the pristine cell. The positive effect of La-incorporation has merited the conductivity of the solar cell; proven through a plunged in R_{ct} from 3100 Ω (pristine cell) to 1200 Ω. The incorporation of La has shortened the carrier lifetime, implies less recombination mechanism and efficient charge carrier transformation from the perovskite layer to the NiO_x. All in all, the PCE of the La-NiO_x perovskite solar cell can still be improved by further modification and more importantly, the addition of La has successfully improved the stability of the perovskite solar cell, which unlocks the opportunity for future commercialization.

Experimental Section

Material Synthesis: All the reagents used in this study were of analytical grade, including 2-methoxyethanol ($H_3COCH_2CH_2OH$, 99.8 %, Wako), diethanolamine $HN(CH_2CH_2OH)_2$, 99.9%, Wako), nickel (II) acetate tetrahydrate ($Ni(OCOCH_3)_2•4H_2O$, 99.999 %, Wako), lanthanum (III) chloride hydrate ($LaCl_3•xH_2O$, 99.999 %, Wako), methylammonium iodide (MAI, $CH_3NH_2•HI$, 99.9 %, Wako), lead (II) iodide (PbI_2, 99.999%, Alfa Aesar), [6,6]-phenyl-C_{61} butyric acid methyl ester ($PC_{61}BM$, >99.5 %, Sigma-Aldrich), N,N-dimethylformamide (DMF, $HCON(CH_3)_2$, 99.8 %, Sigma-Aldrich), Bathocuproine (BCP, 99 %, Wako), dimethyl sulfoxide (DMSO, $(CH_3)_2SO$, >99.9 %, Sigma-Aldrich), chlorobenzene (C_6H_5Cl, 99.8 %, Sigma-Aldrich) and super-dehydrate ethanol were used as-received condition.

NiO_x Based Precursor Solutions: The pristine NiO_x films were synthesized based on the previously reported route.[22] Generally, the 2-methoxyethanol solution containing 0.2 M nickel (II) acetate tetrahydrate and diethanolamine, which acts as a stabilizer and as a ligand to form ionic complexes with the nickel metal was stirred at 70 ºC for overnight to obtain a homogeneous dark green solution, and the solution was then filtered through 45 µm PTFE filters before use. The mole ratio of Ni^{2+} to diethanolamine was maintained at 1:0.012. Whilst, the La-NiO_x films were prepared by mixing various molar ratios (0.5-5.0 mol%) of La with the as-prepared nickel precursor solution and was used for film fabrication.

$CH_3NH_3PbI_3$ Precursor Solution: To prepare a MAI•PbI_2•DMSO adduct solution, 0.2 g MAI and 0.578 g of PbI_2 were dissolved in a mixture solution of DMF:DMSO (ratio 4:1) at room temperature under stirring for overnight to produce a clear and homogeneous yellow solution.[22] The as-prepared precursor solution was filtered with 45 µm PTFE filters and then used for $CH_3NH_3PbI_3$ films fabrication.

Fabrication of Solar Cells: The devices were fabricated on fluorine-doped tin oxide (FTO) glass substrates (15-ohm per square). Initially, the substrates were cleaned sequentially with detergent, deionized water, acetone, and iso-propanol respectively for 15 min in an ultrasonic bath. Then, the cleaned substrates were dried in a moisture-free oven at 150 ºC for 30 min. Finally, UV ozone irradiation under an oxygen-rich condition was performed to remove the organic residue left over the FTO glass substrates to improve the surface wettability. The La-NiO_x HTL was synthesized by spun casting at 3000 rpm for 40 s on the cleaned FTO coated glass substrates at room temperature, subsequently annealed at 450 ºC for 60 min in a muffle furnace with a ramping rate of 3 °C min^{-1}. After that, the substrates were transferred into a nitrogen-filled glove box. For comparison, the pristine NiO_x thin layers were prepared following the same procedure as the La-NiO_x film. Briefly, the perovskite films were fabricated using a simple one-step process where 75 µl of the perovskite precursor solution (MAI•PbI_2•DMSO adduct solution) was pipetted to the HTLs-covered FTO substrates and was spun coated at 4000 rpm for 30 s. 150 µl chlorobenzene anti-solvent was drop-casted during the first 5 s of the spinning process, subsequently, the films were thermally annealed on the hotplate at 100 ºC for 10 min. Next, $PC_{61}BM$ (15 mg ml^{-1} in chlorobenzene) was spin coated on top of the perovskite layer at 1000 rpm for 20 s and 2000 rpm for 10 s. Then, a thin layer of BCP (0.5 mg ml^{-1}) was spin coated on top of the $PC_{61}BM$ layer. Finally, the devices were thermally evaporated with 100 nm Ag as the cathodic electrode using a shadow mask at a pressure of 4 x 10^{-3} torr.

Characterizations: X-ray diffraction (XRD) pattern data was recorded using a (Rigaku Co. Ltd., Tokyo, Japan) X-ray powder diffractometer (40 kV, 40 mA, Cu K*α*, λ = 1.5406 Å). The morphology of the HTL and perovskite layers was captured by field emission scanning electron microscope (FE-SEM) (JSM-6701, JOEL). The surface morphologies were investigated using an atomic force microscopy (AFM) unit in non-contact mode (JSPM-5200, Japan). X-ray photoelectron spectroscopy (XPS) analysis was performed by Shimadzu Kratos AXIS-NOVA spectrometer using monochromatic Al-Kα (1486.6 eV) as the radiation source. The XPS spectra were calibrated by the binding energy of 284.8 eV for C 1s. The Ultraviolet-visible (UV) absorption spectra were recorded using a UV-VIS-NIR spectrophotometer with a wavelength ranging from 300−800 nm at room temperature (V-670, JASCO Co. Ltd., USA). Room temperature static emission spectra and dynamic emission decay spectra were recorded by a spectrofluorometer (HAMAMATSU) where 456 nm pulsed laser was used as an excitation source for the time-resolved PL measurement. Photoelectron yield spectroscopy (PYS) measurement was carried out using Bunkoukeiki KV205-HK ionization energy measurement system with -5.0 V of applied voltage. Electrochemical impedance spectroscopy (EIS) spectra were also obtained using a potentiostat (Solartron Analytical 1255B) in the frequency range of 0.1 Hz to 100 kHz and potentials of 0.8 V under dark conditions. The ZView software was used to analyze the impedance data and the oscillation potential amplitudes were adjusted to 10 mV. The density of state (DOS) was determined using photoelectron yield spectroscopy (PYS) by Bunkoukeiki KV205-HK ionization energy measurement system with an applied voltage of -5.0 V. The voltammogram was obtained using CHI700E (CH Instruments, Inc.) electrochemical workstation under a three-electrode system where pt foil serves as the counter electrode and a standard calomel electrode (SCE) was used as a reference electrode. The Hall measurement was performed using ECOPIA Hall effect measurement system (HMS-3000 VER 3.52). Photovoltaic performances were measured using Bunko Keiki BSOX150LC solar simulator under an illumination power of 100 mW cm^{-2} with an aperture of 0.08 mm^2. The solar simulator was first calibrated with an amorphous Si photodetector (Bunko Keiki BS-520 S/N 353) prior usage. While the incident photon to current efficiency spectra (IPCE) was characterized by using a monochromatic Xenon lamp (Bunkouki CEP-2000SRR).

Acknowledgements

The work was supported by the Grant-in-Aid for Scientific Research (KAKENHI) program, Japan (C, Grant Number 15K05597).

Keywords: Inverted perovskite solar cell; Lanthanum-NiO_x; Hole-transporting layer; High efficiency; Stability

[1] H. J. Snaith, *J. Phy. Chem. Let.* **2013,** *4,* 3623-3630.

[2] B. Saparov, D. B. Mitzi, *Chem. Rev.* **2016**, *116,* 4558-4596.

[3] S. Kazim, M. K. Nazeeruddin, M. Gratzel, S. Ahmad, *Angew. Chem., Int. Ed. Engl.* **2014**, *53*, 2812-2824.

[4] Y. Rong, L. Liu, A. Mei, X. Li, H. Han, *Adv. Energy Mater.* **2015**, *5*, 1501066.

[5] S. S. Mali, H. Kim, S. E. Shim, C. K. Hong, *Nanoscale* **2016,** *8,* 19189-19194.

[6] X. T. Yin, P. Chen, M. D. Que, Y. L. Xing, W. X. Que, C. M. Niu, J. Y. Shao, *ACS Nano* **2016,** *10,* 3630–3636.

[7] Z. Zhu, Y. Bai, T. Zhang, Z. Liu, X. Long, Z. Wei, Z. Wang, L. Zhang, J. Wang, F. Yan, S. Yang, *Angew. Chem. Int. Ed.* **2014,** *53,* 12571–12575.

[8] J. Z. Chen, N. G. Park, *J. Phys. Chem. C,* **2018,** *122,* 14039−14063.

[9] J. W. Jung, C. C. Chueh, A. K. Y. Jen, *Adv. Mater.* **2015**, *27*, 7874-7880.

[10] J. H. Park, J. Seo, S. Park, S. S. Shin, Y. C. Kim, N. J. Jeon, H. W. Shin, T. K. Ahn, J. H. Noh, S. C. Yoon, C. S. Hwang, S. I. Seok, *Adv. Mater.* **2015,** *27,* 4013–4019.

[11] S. Seo, I. J. Park, M. Kim, S. Lee, C. Bae, H. S. Jung, N. G. Park, J. Y. Kim, H. Shin, *Nanoscale* **2016,** *8,* 11403–11412.

[12] B. Wu, H. T. Nguyen, Z. Ku, G. Han, D. Giovanni, N. Mathews, H. J. Fan, *Adv. Energy Mater.* **2016,** *6,* 1600551.

[13] A. Huang, J. T. Zhu, J. Y. Zhang, Y. Yu, Y. Liu, S. W. Yang, S. H. Bao, L. Lei, P. Jin, *J. Mater. Chem. C* **2016,** *4,* 10839-10846.

[14] J. H. Kim, P. W. Liang, S. T. Williams, N. Cho, C. C. Chueh, M. S. Glaz, D. S. Ginger, A. K. Y. Jen, *Adv. Mater.* **2014,** *27,* 695-701.

[15] M. Liu, Z. Zhou, P. Zhang, Q. Tian, W. Zhou, D. Kou, S. Wu, *Opt. Express* **2016,** *24,* A1349-A1359.

[16] I. J. Park, G. Kang, M. A. Park, J. S. Kim, S. W. Seo, D. H. Kim, K. Zhu, T. Park, J. Y. Kim, *ChemSusChem* **2017,** *10,* 2660-2667.

[17] W. Chen, F. Liu, X. Feng, A. B. Djurišić, W. K. Chan, Z. He, *Adv. Energy Mater.* **2017**, 7, 1700722.

[18] W. Chen, Y. Wu, J. Fan, A. B. Djurišić, F. Liu, H. W. Tam, A. Ng, C. Surya, W. K. Chan, D. Wang, Z. He, *Adv. Energy Mater.* **2018**, 8, 1703519.

[19] W. Chen, Y. Zhou, L. Wang, Y. Wu, B. Tu, B. Yu, F. Liu, H. Tam, G. Wang, A. B. Djurišić, L. Huang, Z. He, *Adv. Mater.* **2018**, 30, 1800515.

[20] H. Zhang, X. Ren, X. Wen, J. Mao, J. Cheng, Y. Zhao, Y. Liu, J. Milic, W. Yin, M. Grätzel, W. C. H. Choy, *Energy Environ. Sci.* **2018**, 11, 2253-2262.

[21] J. Zheng, L. Hu, J. S. Yun, M. Zhang, C. F. Jonathan Lau, J. Bing, X. Deng, Q. Ma, Y. Choo, W. Fu, C. Chen, M. A. Green, S. Huang, A. W. Y. Ho-Baillie, *Appl. Energy Mater.* **2018,** *1,* 561-570.

[22] J. Troughton, K. Hooper, T. M. Watson, *Nano Energy* **2017,** *39,* 60–68.

[23] D. X. Yuan, X. D. Yuan, Q. Y. Xu, M. F. Xu, X. B. Shi, Z. K. Wang, L. S. Liao, ***Phys. Chem. Chem. Phys.***, **2015,** ***17,*** 26653-26658.

[24] J. Y. Jeng, K. C. Chen, T. Y. Chiang, P. Y. Lin, T. Da Tsai, Y. C. Chang, T. F. Guo, P. Chen, T. C. Wen, Y. J. Hsu, *Adv. Mater.* **2014**, *26*, 4107-4113.

[25] W. Yu, X. Jiang, S. Ding, B. Q. Li, *J. Power Sources* **2014,** *256,* 440-448.

[26] A. F. Shojaie, M. H. Loghmani, La^{3+} and Zr^{4+} Co-Doped Anatase Nano TiO_2 by Sol-Microwave Method. *Chem. Eng. J.* **2010,** *157,* 263–269.

[27] Y. Tokudome, K. Nakanishi, T. Hanada, *J. Ceram. Soc. Jpn.* **2009,** *117,* 351-355.

[28] X. C. Dou, D. Sabba, N. Mathews, L. H. Wong, Y. M. Lam, S. Mhaisalkar, *Chem. Mater.* **2011,** *23,* 3938–3945.

[29] Z. Liu, A. Zhu, F. Cai, L. Tao, Y. Zhou, Z. Zhao, Q. Chen, Y. B. Cheng, H. Zhou, *J. Mater. Chem. A* **2017**, *5*, 6597-6605.

[30] J. Kim, H. R. Lee, H. P. Kim, T. Lin, A. Kanwat, A. R. bin Mohd Yusoff, J. Jang, *Nanoscale* **2016,** *8*, 9284-9292.

[31] J. You, L. Meng, T. B. Song, T. F. Guo, Y. (Michael) Yang, W. H. Chang, Z. Hong, H. Chen, H. Zhou, Q. Chen, Y. Liu, N. De Marco, Y. Yang, *Nat. Nanotechnol.* **2016**, *11*, 75-81.

[32] J. Mo, C. Zhang, J. Chang, H. Yang, H. Xi, D. Chen, Z. Lin, G. Lu, J. Zhang, Y. Hao, *J. Mater. Chem. A* **2017,** *5,* 13032-13038.

[33] Y.C. Wang, J. Chang, L. Zhu, X. Li, C. Song, J. Fang, *Adv. Funct. Mater.* **2018**, *28*, 1706317.

[34] Y. Wu, W. Chen, Y. Yue, J. Liu, E. Bi, X. Yang, A. Islam L. Han, *ACS Appl. Mater. Interfaces* **2015,** *7,* 20707-20713.

[35] W. Chen, G. N. Zhang, L. M. Xu, R. Gu, Z. H. Xu, H. J. Wang, Z. B. He, Mater. *Today Energy* **2016,** *1–2,* 1-10.

[36] J. Chang, H. Zhu, B. Li, F. Isikgor, Y. Hao, Q. Xu, J. Ouyang, *J. Mater. Chem. A* **2016**, *4*, 887-893.

[37] Y. Diamant, S. G. Chen, O. Melamed A. Zaban, *J. Phys. Chem. B* **2003,** *107,* 1977-1981.

[38] L. L. Jiang, Z. K. Wang, M. Li, C. C. Zhang, Q. Q. Ye, K. H. Hu, D. Z. Lu, P. F. Fang, L. S. Liao, *Adv. Funct. Mater.* **2018,** *28,* 1705875.

[39] G. Kapil, T. S. Ripolles, K. Hamada, Y.Ogomi, T. Bessho, T. Kinoshita, J. Chantana, K. Yoshino, Q. Shen, T. Toyoda, *Nano Lett.* **2018,** *18,* 3600-3607.

[40] W. Chen, L. Xu, X. Feng, J. Jie, Z. He, *Adv. Mater.* **2017**, *29*, 1603923.

[41] W. Chen, Y. Wu, Y. Yue, J. Liu, W. Zhang, X. Yang, H. Chen, E. Bi, I. Ashraful, M. Gratzel, L. Han, *Science* **2015**, *350*, 944-948.

Entry for the Table of Contents

FULL PAPER

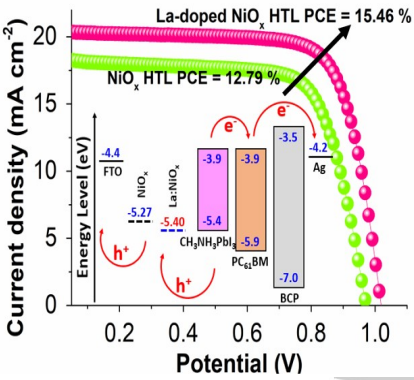

Siowhwa Teo,[a] Zhanglin Guo,[a] Zhenhua Xu,[a] Chu Zhang,[a] Yusuke Kamata,[a] Shuzi Hayase,[a] Tingli Ma*[a]*

Page No. – Page No.

The role of lanthanum on a nickel oxide-based inverted perovskite solar cell for efficiency and stability improvement

The perovskite solar cell, with La-NiO$_x$ as the HTL, exhibits 21% enhancement in efficiency and a remarkable stability than that of pristine NiO$_x$ owing to the effectiveness of small amount of La in passivating defects states.